Surface Design based on Geometric Flow Method and Tessellation

Haogui CHEN
Hunan City University, Yiyang, Hunan 413000, CHINA

Abstract: This paper combines geometric flow method with tessellation and make full use of their respective strengths to complete some surface design problems, such as surface blending, N sides fill holes and others which satisfy G1 boundary conditions. Based on full analysis of subdivision, the technology utilizes the discrete of four-order geometric flows to successfully construct four-order geometric partial differential equations' finite element method based on quadrilateral surface subdivision. Experimental results show that: surface design which based on geometric flow method and surface subdivision is effective and correct.

Keywords: Discrete; Surface blending; Geometric partial differential equations; Diffusion flow

1. Introduction

In surface design, Bloor and others first proposed surface construction method based on partial differential equations. After that the method which based on PDE develops rapidly and it is widely used in computer-aided surface design. Later, it is proposed to use the geometric PDE method to construct surfaces. For example, the mean curvature flow is a second-order geometric PDE, which has good smoothness and noise canceling features, has been successfully applied in the design of the smooth surface, curved stitching and free surface design and other issues. In recent years, surface design method based on fourth-order geometric PDE has became a hot topic in the field, for it can generate G1 continuous stitching surface. All the above methods are represented with the discrete grid method of surface. As the B-spline, NURBS emerge and develop, the spline surface representation is gradually introduced into the surface design. Earlier, Bloor and others applied B-spline as the solution of biharmonic equation.Later, Terzopoulos etc., put forward a dynamic NURBS method, using a second-order differential equation to determine the evolution of DNURBS [1-3]. But the equation is not intrinsic geometry and can not get NURBS' G1 smooth stitching.

Surface design has been formed a theoretical system which takes NURBS parametric feature technology and implicit algebraic surfaces as the main body, takes interpolations, fitting, approaching as the skeleton. As computer graphics requirements for the authenticity of objects increase, the object's geometric design complexity increases and research areas the expands, using only parametric polynomial has been far from able to satisfy demand, it is urgent to call for new ways to solve new problems that appear in various research areas. So segmentation techniques, partial differential equations methods have been widely applied to these emerging field of study [4].

As we all know, three-dimensional data sampling techniques and hardware devices rapidly develop, such as laser range scanning, object's initial mesh can be easily generated on the computer; more importantly, because the graphics industry's demand for smooth surface modeling of arbitrary topology is increasingly urgent, the traditional Bézier, B-spline methods can not meet the requirements any more, they have serious limitations in design of arbitrary shaped boundaries and surfaces of arbitrary topology, while tessellation is able to provide a simple and efficient algorithm to characterize arbitrary topology free-form surfaces, and has a certain order of smoothness. In 1974, Chaikin first proposed the concept of discrete segments [4]. In 1978, Doo Catmull etc., put forward subdivision rules of biquadratic and Bi-cubic tensor product B-spline surfaces based on quadrilateral meshes [5-7].

2. Thought of Subdivision

Subdivision method is a discrete modeling approach gradually developed since the late 1974s and was considered geometric modeling industry as one of the key technologies for the next generation of geometric modeling. The basic idea generated from the free surface modeling technology in the early 1970s. As shown in Figure 1, control polygon of cubic *B.zier* curve is $\eta = [q_0, q_1, q_2, q_3]$.Mapping method or the de Casteljau algorithm can obtain a point $q_3^{'}\left(q_3^{'} = q_0^{'}\right)$ on the curve B□zier. $q_3^{'}$ divides the curve into two child cubic *B.zier* curves which take $\eta = \left[q_0^{'}, q_1^{'}, q_2^{'}, q_3^{'}\right]$ and $\eta = [q_0, q_1, q_2, q_3]$ as the control polygon .Obviously, the

broken line combined by the control polygon η_1 and η_2 is more approximate to *B.zier* curve than η. If repeat the segmentation process on curves of η_1 and η_2, broken line which is more approximate to *B.zier* curve can be got. If the iterative process continues, the resulting line will rapidly converge *B.zier* curve.

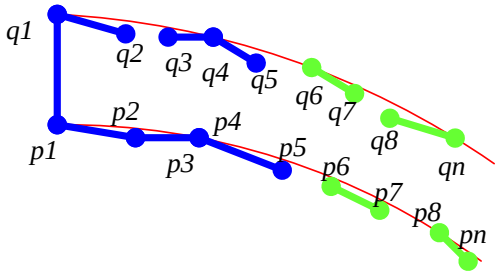

Figure 1. One time subdivision of the cubic B ⌊zier curve

Segmentation model discussed in this article is the popularization of the above subdivision thought in the space triangular control grid, first proposed by Loop of Utah University in the United States, the resulted surface is promotion of the box-spline surfaces.

For non-triangular meshes (like quadrilateral mesh), triangulation is required before subdivision. On a triangle conduct one Loop subdivision can generate four sub-triangles (as Figure 2), the vertexes of the triangle can be divided into sub-parent triangular top bit (vertex-point) and edge points (edge-point). The former is subdivided from the parent triangle vertexes before changing, as $[q_0', q_1', q_2']$ in Figure 2; the latter is new vertex generated from triangle edge of the parent by the segmentation process, such as q_1, q_2, q_3. Vertex-point and edge points are generated by the parent triangle vertexes and directly adjacent vertexes in the grid by using vertex template and edge template by affine combinations.

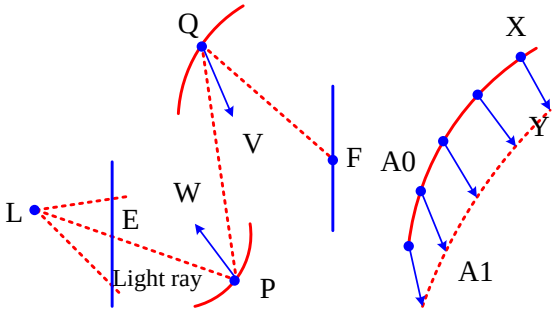

Figure 2. Triangle 1- 4 schematic subdivision

As shown in Figure 3, for vertexes $q_0^{(l)}$ with degree on l (l = 0,1,2, ...) subdivision level , supposed that directly adjacent vertexes in the mesh is $q_0^{(l)}, q_1^{(l)}, q_2^{(l)}, q_n^{(l)}$, then new location $q_0^{(l+1)}$ of the vertex $q_0^{(l)}$ on $l+n$ level and directly adjacent vertexes $q_i^{(l+1)}\ (i=1,...,n)$ can be obtained by using the following vertex-point / side point rules.

$$w_0(n) = n / a(n) - n$$
$$a(n) = \frac{5}{8} - \left[3 + 2\cos(2\pi / n)\right]^2 / 128 \quad (1)$$

Use the above rules to conduct subdivision iteration on triangular mesh and control grid, then a smooth limit surface will be converged. Each vertex v of initial control mesh can find a corresponding point $v\infty$ on the limit surface . *M.uller* etc,. put forward the formula to strike $v\infty$ and its two non-collinear cut vectors u1 and u_2 on limit surface, then normal direction of surface at $v\infty$ point can be obtained .

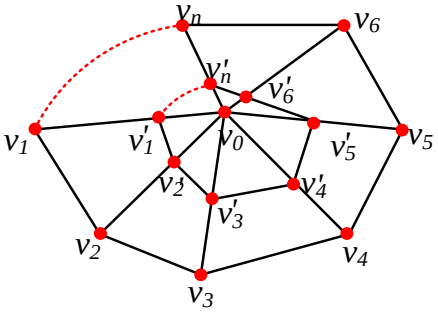

Figure 2. Generation of triangular mesh point and its adjacent vertexes on l+1 subdivision hierarchy

Boundary treatment, edit and modification of curves are as follows:

Conduct respectively once and twice subdivision o the initial grid. It is not difficult to find that the subdivided grid is also dense in where the initial control triangle network is dense; relatively straight edges of control network on plowshare site become jagged after subdivision ; The outer edge of the wing plow and the edge of plows chest are not smooth, which are not expected. Its main causes are that subdivision rules are used for vertex-point and edge point on the border of the grid and inside the grid during subdivision.

In order to eliminate the affect of subdivision process on the geometric properties of control mesh boundary, it is necessary to modify the generation rules for the vertex point and edge point of boundaries.

It is needed to respectively treat borders that maintain smooth and straight, mark respectively the initial mesh vertexes .For the former, the boundary vertex point just needs to remain unchanged, and the boundary edge point only needs to do linear interpolation on the end points of the edge; The latter, in order to make the surface smooth at the boundary point, it needs to modify the weight of the vertex point and edge point template which take the boundary points as end points and the inner side edge

point template, the modified rules are shown in Figure 4.Among which,

$$k_1 = 1/4 \quad k_2 = 1/2$$

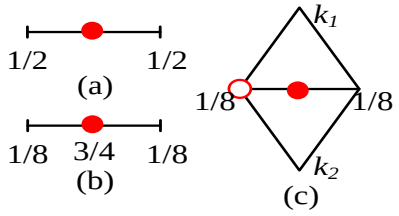

Figure 3. Templates of vertex points and edge points in modified grid boundary vertex

More generally, the boundary control method is to introduce a normal into the grid. Normal control can achieve an arbitrary boundary surface control by changing the size of the right of boundary points' subdivision rule, and through the subdivision process control mesh can be generated from the original breakdown of the various resolution mesh model. These grid models can be used as input of finite element calculation or dynamic simulation software, through the establishment of soil plow surface movement along mattress mechanical model. By conducting finite element calculation or simulation on the plow surface under different tillage speeds, tillage depth, soil deformation and soil condition mattress and other conditions of work performance and efficiency, the basis for the design of complex plow surface can be provided.

3. Equation Model and its Weak Form

Equation models of surface diffusion flow, Willmore flow and surface diffusion flow are listed below. Let S be a closed orientable surface of R_3, it is needed to find a family of smooth and orientable surface set $\{s(t): t \geq 0\}$, which meet below conditions:

$$W(S) := \int_S R^2 d\sigma \tag{2}$$

Proposed surface diffusion flow

$$\begin{cases} \dfrac{\partial x}{\partial t} = -\Delta_s^2 x, \ S(0) = S_0 \\ \partial S(t) = \Gamma \end{cases} \tag{3}$$

This paper adopts mixed finite element method to solve these three four order geometric flows, control vertexes on the surface are the unknown quantity need to be determined , the average surface curvature and mean curvature vector are also treated as unknown quantities. Specific steps are as follows: First, the fourth-order equations are written in two second-order equations coupled system; Then create this coupled system variational form(weak form), then conduct the discretization of finite element , exporting a linear system; finally use iterative method to solve the linear system to obtain approximate solutions.

The following are their weak forms, let the trial function φ , $\forall \phi \in R^I(S)$,then formula (9) (10) weak forms as follows: find $\forall \varphi \in R^I(S)$,which makes

$$\begin{cases} \int_s \dfrac{\partial x}{\partial t} \phi dA + 2\int_s [\phi \varnothing R - n(\nabla_s \phi)^T \nabla_s R] dA = 0, \\ \forall \phi \in R^I(S) \\ \int sR\varphi dA - \dfrac{1}{2}\int_s tr(\varnothing x)\varphi dA = 0, \forall \varphi \in R^I(S) \end{cases} \tag{4}$$

And

$$\begin{cases} \int_s \dfrac{\partial x}{\partial t} \phi dA + \int_s [\phi \varnothing R - n(\nabla_s \phi)^T \nabla_s R] dA + \\ \int_s 2n(R^2 - K)\phi R dA = 0, \forall \phi \in R^I(S) \\ \int_s R\varphi dA - \dfrac{1}{2}\int_s tr(\varnothing x)\varphi dA = 0, \forall \varphi \in R^I(S) \end{cases} \tag{5}$$

Weak form of formula (11) is as: find $\forall \varphi \in R^I(S)$, which makes

$$\begin{cases} \int_s \dfrac{\partial x}{\partial t} \phi dA - 2\int_s \nabla sR \nabla s \phi dA = 0, \forall \phi \in R^I(S) \\ \int_s R\varphi dA + \dfrac{1}{2}\int_s (\nabla sx)^T \nabla s \varphi dA = 0, \forall \varphi \in R^I(S) \end{cases} \tag{6}$$

4. Discrete of Four Order Geometric Flows

Equation's finite element discretization will be described as below. First, introduce two finite element space $E_r = span[\Omega_1, \Omega_2, ...\Omega_n]$ and $F_r = span[\Omega_1, \Omega_2, ...\Omega_n]$. In E_r and F_r, carry out spatial discrete for the control vertex x, mean curvature H and mean curvature normal R. Let T be a quadrilateral control mesh of surface s, its control vertex is denoted as $\{x_j\}_{i=1}^{n}$. Classification of the control vertexes is provided in the following. The first category are interior vertexes , whose location are unknown and they are the amount to be solved in this paper , denoted as $\{x_j\}_{i=1}^{n_0}$.For curved stitching or N-sided hole filling problem, it requires internal vertexes in stitching or patching area. The rest of the control vertexes are denoted as $\{x_j\}_{i=n_0+1}^{n}$, they are known quantity. Continue to carry on classification. Denote vertex which is adjacent to internal vertex $\{x_j\}_{i=1}^{n_0}$ as $\{x_j\}_{i=n_2+1}^{n_2}$ within two circles. Then the remaining vertexes are denoted as $\{x_j\}_{i=n_2+1}^{n_0}$, the mean curvature of these vertexes is known. So unknowns need to be solved is the position $\{x_j\}_{i=1}^{n_0}$ of the

control vertex, mean curvature $\{R_i\}_{i=1}^{n_2}$ and mean curvature vector $\{R_i\}_{i=1}^{n_2}$ can be written as

Wherein $R_j(t)$ and $R(t)$ respectively represents the mean curvature and the mean curvature vector at the vertex x_j. In this paper, basis functions Ω_j and η_j of each vertex x_j are all limit function form of Catmull-Clark subdivision format, the value at the control point x_j is 1, the value is 0 at the other points. Branched groups of Ω_j and η_j are local, including the vertexes within 2 circles around control point x_j. In actual calculation, the parameter value is taken as a unit within the quadrilateral Gauss nodes. If vertex x j is non-rule-based, partial subdivision can be carried out in its vicinity until Gauss point parameter values fall into a regular bi-cubic B-spline surface chip.

Put the discretization form formula (7) (8) of control vertex x and mean curvature H in the finite element space into equation (4) (5), taking the trial function $\{\Omega\}_{i=1}^{n_0}$ and $\{\Omega\}_{i=1}^{n_2}$, by the known condition it can be known that $\beta x_j(t)/\beta_t = 0$ (when $j \succ n_0$, x_j is fixed). Then put the items which are relative to the known control vertex $\{x_i\}_{i=n_0+1}^{n}$ and the mean curvature $\{R_i\}_{i=n_2+1}^{n}$ to the right side of equation, then get matrix form of formula (4) (5) as the following

$$\begin{cases} M_{n_0}^{(1)} \dfrac{\partial X_{n_0}(t)}{\partial t} + L_{n_2}^{(1)} Y_{n_2}(t) = B^{(1)} \\ M_{n_2}^{(2)} Y_{n_2}(t) + L_{n_0}^{(2)} X_{n_0}(t) = B^{(2)} \end{cases} \quad (7)$$

The elements of which are defined as follows:

$$m_{ij}^{(1)} = [\int_s \phi_i \phi_j dA] I_3, m_{ij}^{(2)} = \int_s \varphi_i \varphi_j dA;$$

$$l_{ij}^{(1)} = \begin{cases} 2\int_s [\phi_i \varnothing \varphi_j - n(\nabla s\varphi_j)^T \nabla s\varphi_j] dA, \text{ for SDF} \\ \int_s [\phi_i [\varnothing \varphi_j + 2n(H^2 - K)\varphi_j] - n(\nabla s\phi_i)^T \nabla s\varphi_j] dA, \text{ for WF} \end{cases}$$

$$l_{ij}^{(2)} = -\frac{1}{2}\int_s [\varphi_i (\varnothing \phi_j)^T - (\nabla s\varphi_i)^T \nabla s\phi_j n^T] dA \quad (8)$$

The dimension of the right hand side are $C(1) \in R_3 n_0$, $C(2) \in Rn_2$.

Similarly, put equation (15) (16) into equation (8), similarly, matrix form of formula (18) is as

$$m_{ij}^{(3)} = \int_S \phi_i \phi_j dA, m_{ij}^{(4)} = \int_S \varphi_i \varphi_j dA;$$
$$l_{ij}^{(3)} = -2\int_S (\nabla s\varphi_j)^T \nabla s\phi_i dA, \quad (9)$$
$$l_{ij}^{(4)} = \frac{1}{2}\int_S (\nabla s\phi_j)^T \nabla s\varphi_i dA.$$

The dimension of the right hand side are $C(3) \in Rn_0 \times 3$, $C(4) \in Rn_2 \times 3$.

In the following conduct time discretization. For formula (18), assuming there areapproximate solution $x_{n_0}^{(k)} = x_{n_0}(t_k)$ and $x_{n_2}^{(k)} = x_{n_2}(t_k)$ when time $t = t_k$. Semi-implicit Euler scheme can be used to construct the approximate solution $x_{n_0}^{(k+1)} = x_{n_0}(t_k + 1)$ and $x_{n_2}^{(k+1)} = x_{n_2}(t_k + 1)$ when $t = t_{k+1} = t_k + \tau(k)$, namely use $[x_{n_0}(t_{k+1}) - x_{n_0}(t_k)]/\tau^{(k)}$ to replace the derivative $\partial X_{n_0}(t)/\partial t$, surface data when $t = t_k$ is used to calculate matrix $M(1)$, $M(2)$, $L(1)$ and $L(2)$ of formula (19).

Then result in a linear system for solving $x_{n_0}^{(k+1)}$ and $x_{n_2}^{(k+1)}$.

$$\begin{bmatrix} M_{n_0}^{(1)} & \tau^{(k)} L_{n_2}^{(1)} \\ L_{n_0}^{(2)} & M_{n_2}^{(2)} \end{bmatrix} \begin{bmatrix} X_{n_0}^{(k+1)} \\ Y_{n_2}^{(k+1)} \end{bmatrix} = \begin{bmatrix} \tau^{(k)} B^{(1)} + M_{n_0}^{(1)} X_{n_0}^{(k)} \\ B^{(2)} \end{bmatrix} \quad (10)$$

Noted that although $M(1)$ and $M(2)$ of the coefficient matrix is symmetric positive definite, but the overall coefficient matrix is not symmetric positive definite. In this paper, the GMRES iterative method proposed by s a a_d is used to solve the system.

5. Simulation and Analysis

This section presents several numerical examples to illustrate QSDF, SDF and WF'S different surface evolution effects, and how to use them to solve some problems of surface design.

5.1. Effects of SDF, ASDF and WF

All four order equations have surfaces polished or denoising function, as can be seen from Figure 5, three short-term four order stream's evolution effect is similar, but the long-term evolution effect is significantly different.

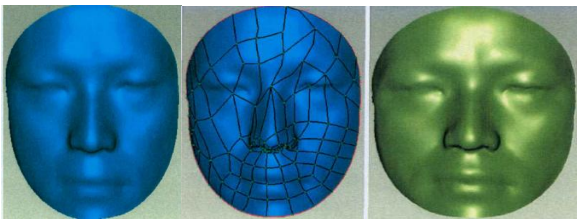

Figure 5. Effect comparison of SDF, QSDF and WF

In Figure 5, from left to right the first is an input surface mesh, the second and third one are respectively the results after twice and four times evolutions through QSDF. The fourth and the fifth one are the results are respectively the results after four times and seven times evolutions through QSDF and time step length is taken as 0.00005.

As can be seen, since SDF has a volume-preserving nature, it can remain initial surface shape better than QSDF and WF, so SDF is more suitable for solving the problem of smooth surface. In addition, QSDF can rapidly shrink surface, while WF expands the surface. Therefore, according to the actual need to select the appropriate geometric flow, the three streams' different evolutionary effects can also be reflected in the splicing problems.

5.2. Blending surfaces

Given a set of boundary surface mesh, it needs to construct a smooth transition surface to stitch together the given surface and has G_1 continuity at the stitching boundary. In Figure 6, the surfaces to be spliced are cylinders of three mutually perpendicular surfaces , as shown in Figure 6a, Figure 6b shows an initial mosaic surface with smooth G_0 , Figure 5c shows the result of the evolution through QSDF; Figure 6d shows the results of evolution through SDF; Figure 6e shows the result of evolution through WF. Except the first line model in Figure 6c, all other images are the results after 100 iterations, the time step is taken to be 0.0113. Due to the QSDF area reduction effect, further iteration will be singular, first line model in Figure 6c is the result after 64 iterations. These figures clearly show the G_1 smoothness at the splicing boundaries and the difference between the effect of evolution. QSDF Surface is more contracted than SDF surface, while WF surface is more expanded than SDF surface. This effect is consistent with Figure 1. In Figure 6, the three cylinders of the second line model are thicker than that of the first line model. It can be known that SDF has volume-preserving properties, WF has a swelling effect, while QSDF is area-reducing. Therefore, when the area to be filled is large, the effects of these geometric flows will be clearly reflected (like the first row models in Figure 6); if the area to be filled is small, the evolution difference is very small. Compared to the first row in Figure 5, there is no significant blending surface difference of the three four order streams in the second row.

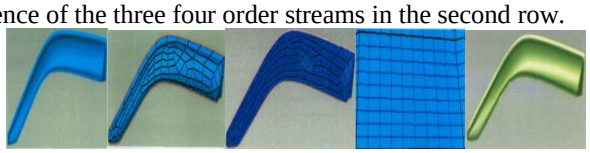

(a) (b) (c) (d) (e)

Figure 6. Blending Surfaces

5.3. Side fill holes

Given surface mesh with holes, it is needy to construct the surface patches with G_1 smooth on boundary. Figure 7 shows an frog model of N-sided hole filling. Figure 7c shows the restored surfaces after 2 iterations by using WF, the time step length is 0.00001. SDF and QSDF's evolution results are similar.

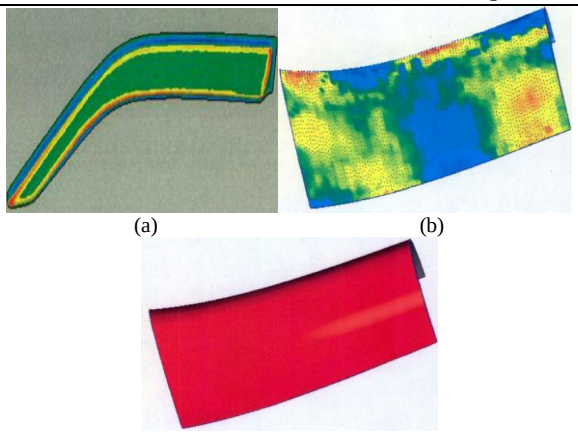

(a) (b)

(c)

Figure 7. Frog model with N side filling hole

5.4. Examples verification

Example 1: Given the control point matrix $matrix\left(p_{ij}\right)^{2\times 2}$ of the surface:

$$\begin{bmatrix} (-1,-1,0) & (-1,0,1) & (-1,1,0) \\ (0,-1,1) & \text{Unknown} & (0,1,1) \\ (1,-1,0) & (1,0,1) & (1,1,0) \end{bmatrix}$$

At this point, $i=k=h=n=m=4$, B-spline surface is a pair of quadric surfaces with 33 control vertexes . Wherein, the required internal control point is just a p_{20} , so that equation (1) contains only one formula. By the program it can be calculated that the unknown internal control vertexes are $p_{20}=(0,0,0.6)$, so that the required uniform surface can be drawn out , as shown in Figure 8. The surface area is 4.213, the maximum absolute value of mean curvature surface is 1.701 and the average value is 0.791.

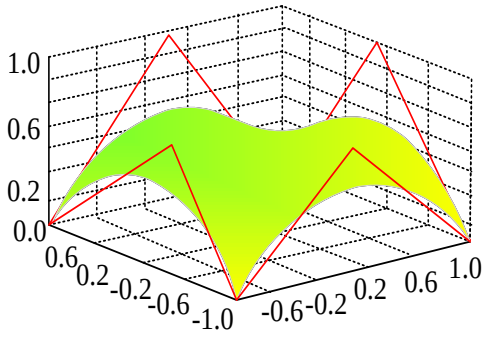

Figure 8. Surface that contains only one internal control vertex

Example 2: Given the control point matrix $matrix\left(p_{ij}\right)^{3\times 3}$ of the desired surface:

$$\begin{bmatrix} (-1,-1,0) & (-1,-0.5,0.5) & (-1,0.5,0.5) & (-1,1,0) \\ (-0.5,-1,0.5) & \text{Unknown} & \text{Unknown} & (-0.5,1,0.5) \\ (0.5,-1,0.5) & \text{Unknown} & \text{Unknown} & (0.5,1,0.5) \\ (1,-1,0) & (1,-0.5,0.5) & (1,0.5,0.5) & (1,1,0) \end{bmatrix}$$

Use bi-quadratic uniform B-spline surfaces to design, i,e , $i=h=4$, $n=m=4$, the number of control vertexes is 44. Among them, there are four required internal control vertexes, so the formula (20) contains four equations, we can calculate the four internal control vertexes:

$$P_{22}=(-0.5,-0.5,0.375), P_{23}=(-0.5,0.5,0.375),$$

$$P_{32}=(0.5,-0.5,0.375), P_{33}=(0.5,0.5,0.375).$$

The obtained B-spline minimal surfaces are shown in Figure 9. The surface area is 4.125, the maximum absolute value of mean curvature surfaces is 6 and the average value is 1.413.

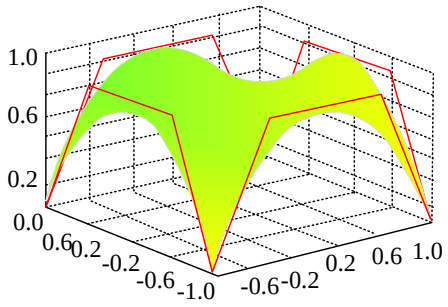

Figure 9. Surface that contains four internal control vertexes

6. Conclusion

Tessellation technology provides a simple and efficient way to construct arbitrary topology and at the same time has a certain order of smoothness of the surface. Geometric method is a powerful technology for constructing high-quality surfaces. This article organically combines the two together and give full play to the advantages of both, in a unified framework it solves some surface design problems such as surface blending, N side fill holes and others which meet G_1 boundary conditions. This paper has successfully constructed the finite element method for surfaces of four order geometric partial differential equations based on quadrilateral Catmull-Clark subdivision.

References

[1] Xin Huang, Xiao Ma, Bangdao Chen, Andrew Markham, Qinghua Wang, Andrew William Roscoe. Human Interactive Secure ID Management in Body Sensor Networks. Journal of Networks, Vol 7, No 9 (2012), 1400-1406

[2] Ramesh Raskar, Immersive planar display using roughly aligned projectors. New York, USA, Proceedings of IEEE Virtual Reality, 2000.

[3] Chen Y, Clark D W.' Automatic alignment of high-resolution multi-projector displays using an un-calibrated camera, IEEE Visualization, 2000.

[4] Jannick P. Rolland and Kevin P. Thompson, Freeform optics: Evolution? No, revolution SPIE Newsroom 10.1117/2.1201207.004309, pp: l-3, 2012.

[5] Vu Q H, Ooi B C, Rinard M, et al. Histogram-based global load balancing in structured peer-to-peer systems. Knowledge and Data Engineering, IEEE Transactions on, 2009, 21(4): 595-608.

[6] Hsiao H C, Liao H, Chen S T, et al. Load Balance with Imperfect Information in Structured Peer-to-Peer Systems. Parallel and Distributed Systems, IEEE Transactions on, 2011, 22(4): 634-649.

[7] Jones P, EASTLAKE D E. US secure hash algorithm 1 (SHA1). 2001:902-910